ADVANCED MATERIALS

www.advmat.de

Check for updates

Few-Layer GeAs Field-Effect Transistors and Infrared Photodetectors

Jian Guo, Yuan Liu, Yue Ma, Enbo Zhu, Shannon Lee, Zixuan Lu, Zipeng Zhao, Changhao Xu, Sung-Joon Lee, Hao Wu, Kirill Kovnir, Yu Huang, and Xiangfeng Duan**

The family of 2D semiconductors (2DSCs) has grown rapidly since the first isolation of graphene. The emergence of each 2DSC material brings considerable excitement for its unique electrical, optical, and mechanical properties, which are often highly distinct from their 3D counterparts. To date, studies of 2DSC are majorly focused on group IV (e.g., graphene, silicene), group V (e.g., phosphorene), or group VIB compounds (transition metal dichalcogenides, TMD), and have inspired considerable effort in searching for novel 2DSCs. Here, the first electrical characterization of group IV–V compounds is presented by investigating few-layer GeAs field-effect transistors. With back-gate device geometry, p-type behaviors are observed at room temperature. Importantly, the hole carrier mobility is found to approach 100 cm^2 V^{-1} s^{-1} with ON–OFF ratio over 10^5, comparable well with state-of-the-art TMD devices. With the unique crystal structure the few-layer GeAs show highly anisotropic optical and electronic properties (anisotropic mobility ratio of 4.8). Furthermore, GeAs based transistor shows prominent and rapid photoresponse to 1.6 µm radiation with a photoresponsivity of 6 A W^{-1} and a rise and fall time of ≈3 ms. This study of group IV–V 2DSC materials greatly expands the 2D family, and can enable new opportunities in functional electronics and optoelectronics based on 2DSCs.

With the discovery and rapid rise of graphene, 2D layered materials (2DLMs) were rapidly enriched by rediscovering atomic thin properties of well-studied layered bulk crystals,[1] such as black phosphorus[2,3] and as MoS_2.[4] Among many 2DLMs, 2DSCs are highly attractive for their highly tunable bandgap,[5,6] atomic thin body,[7] and superior immunity to short channel effects.[8–10] For example, with a body thickness $t_{body} < 1$ nm, layered MoS_2 shows smaller gate screening length ($\lambda \approx t_{body}^{0.5}$)[11] and larger bandgap (1.9 vs 1.1 eV)[12] compared to silicon, both of which will suppress short channel effects and reduce power dissipation.[13] Layered black phosphorus exhibits high carrier mobility $\mu > 1000$ cm^2 V^{-1} s^{-1}[14] at room temperature, in contrast to the poor electrical performance of silicon ($\mu < 500$ cm^2 V^{-1} s^{-1})[15] when shrinking down to 5 nm body thickness. Importantly, the dangling-bond-free surface[16] and weak van der Waals (vdW) interaction[17] in 2DSC ensures excellent electronic properties and great flexibility in terms of 2DSC growth,[18] dielectric deposition, and substrate integration without the traditional constraints of lattice mismatch[19] and other material incompatibilities. These promising properties have intrigued continuous searching for novel 2DSCs. Recent theoretical studies[20,21] have revealed another large family of 2DSCs with tunable bandgap, which includes IV–V group compound germanium and silicon monopnictides (e.g., GeAs and SiAs). Although early studies have inspected their lattice structure,[21] bandgap,[20] Hall mobility,[22] and thermoelectric performance[23] in bulk crystals, there are no reports of electrical properties based on few-layer flakes. Here, we report, for the first time, the semiconducting electronic properties of 2D GeAs. With a back-gate geometry, few-layer GeAs transistors show high ON-OFF ratio of 10^5 and maximum hole field-effect mobility of 99 cm^2 V^{-1} s^{-1} at room temperature, comparable with that of transition metal dichalcogenides (TMD) materials. We also observe highly angle dependent optical and electronic properties in GeAs flakes. To reveal the intrinsic electronic properties of multilayer GeAs, metal and semiconductor contact was systematically studied by examining the Schottky barrier height and temperature dependent contact resistance (R_C). The extracted intrinsic mobility implies charged impurity scattering limited transport of GeAs at low temperature. Taking advantage of the narrow band gap of multilayer GeAs, we demonstrate GeAs-based

J. Guo, Dr. Y. Liu, Y. Ma, E. Zhu, S. Lee, Z. Lu, Z. Zhao, C. Xu, S.-J. Lee, H. Wu, Prof. Y. Huang
Department of Materials Science and Engineering
University of California
Los Angeles, CA 90095, USA
E-mail: yhuang@seas.ucla.edu

S. Lee, Prof. K. Kovnir
Department of Chemistry
Iowa State University, and Ames Laboratory
Ames, IA 50011, USA

Prof. X. Duan
Department of Chemistry and Biochemistry
University of California
Los Angeles, CA 90095, USA
E-mail: xduan@chem.ucla.edu

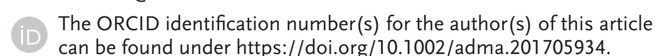
The ORCID identification number(s) for the author(s) of this article can be found under https://doi.org/10.1002/adma.201705934.

DOI: 10.1002/adma.201705934

© 2018 WILEY-VCH Verlag GmbH & Co. KGaA, Weinheim

15214095, 2018, 21, Downloaded from https://onlinelibrary.wiley.com/doi/10.1002/adma.201705934 by California Inst of Technology, Wiley Online Library on [30/12/2023]. See the Terms and Conditions (https://onlinelibrary.wiley.com/terms-and-conditions) on Wiley Online Library for rules of use; OA articles are governed by the applicable Creative Commons License

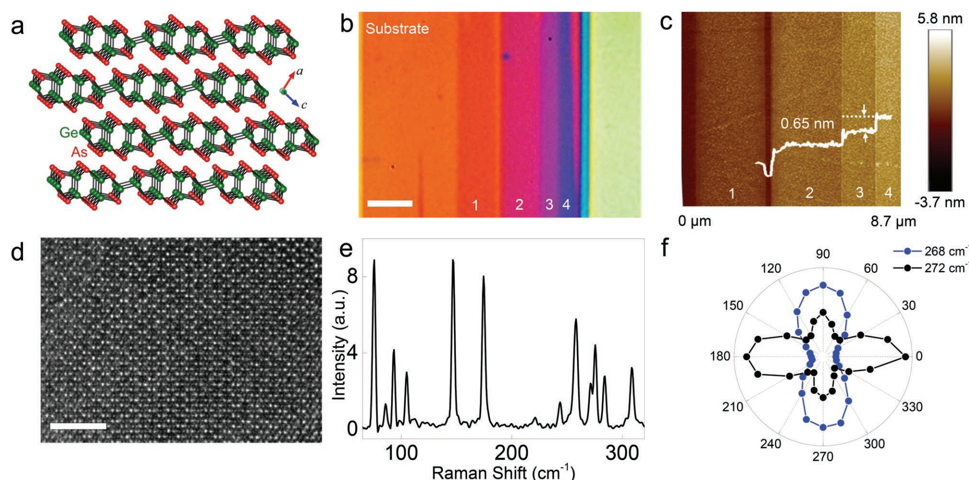

Figure 1. Crystal structure, schematics and material characterization. a) Schematics of GeAs crystal structure. b) Optical image of ultrathin GeAs flakes on SiO_2 substrate. Numbers from 1 to 4 mark the number of layers for each flake. The scale bar is 5 µm. c) AFM image of corresponding GeAs flakes (in b), which demonstrates atomic thin flakes with the number of layer from 1 to 4 as indicated. d). High resolution TEM image of GeAs atomic layers. Scale bar is 3 nm. e) Raman spectrum of multilayer GeAs flake using 633 nm polarized laser excitation. f) Polar plot of angle-resolved Raman spectrum at peak 268 and 272 cm^{-1}, which demonstrates highly anisotropic characteristic.

mid-infrared photodetector with considerable responsivity and fast response time. Our study here not only demonstrates a new promising 2DSC, but also expands the 2D family to group IV–V compounds that are more closely related to traditional group IV (e.g., Si, Ge) and group III–V semiconductors (e.g., GaAs).

Crystal structures of GeAs bulk crystals have been well studied theoretically. Briefly, GeAs bulk crystalizes in layered GaTe structure type in the space group $C2/m$ (No. 12).[24] As illustrated in **Figure 1**a, within each layer, Ge atoms (green) bond with one Ge atom and three As atoms (red), forming distorted $As_2@Ge_6$ octahedra. Each GeAs layer is terminated by As atoms and interacts with others by weak van der Waals forces. Interestingly, two types of Ge—Ge bonds are clearly distinguishable in the crystal structure: one type is parallel and the other one is perpendicular to the layer plane, which demonstrates anisotropic nature of GeAs crystal structure. To experimentally identify the layered structure of GeAs crystal, atomic thin GeAs film was peeled onto a SiO_2 substrate by micromechanical exfoliation and was then examined by optical microscope and atomic force microscope (AFM). The optical image in Figure 1b shows several ultrathin GeAs stripes successfully obtained on SiO_2 substrate, which present distinct optical contrast. Further study of corresponding height profile in AFM image (Figure 1c) identifies single, double, triple and four layers of GeAs flakes, which are marked by numbers 1–4 in both optical and AFM image. The height profile also gives a typical layer spacing of GeAs flakes around 0.65 nm, which is similar to those of TMDs. High resolution transmission electron microscopy (HRTEM) is then utilized to examine GeAs atomic structure. Through a proper zone axis (toward plane (25, 0, −11)), slightly distorted hexagonal structures (bright white dots) are observed (Figure 1d), which are projections of the vertically aligned As atoms and Ge atoms.

Raman spectroscopy is widely exploited as a fingerprint for identifying materials and powerful tool for determining crystal symmetries. A typical Raman spectrum of a multilayer GeAs flake shows multiple peaks due to highly asymmetric structure (Figure 1e). Two of the most intense peaks (167 and 220 cm^{-1}) correspond to atomic vibrations perpendicular to the *b*-axis.[25] Angular-resolved polarized Raman spectrum is then measured. The polar plot of Raman peak at 268 cm^{-1} shows anisotropic variation period of 180°, while the peak at 272 cm^{-1} reach the maximum intensities by 90° spacing (Figure 1f). To match the anisotropic Raman spectrum and crystal orientation, we examine the corresponding HRTEM image (Figure S1a,b, Supporting Information), which suggests that the maximum intensity of peak at 272 cm^{-1} corresponds to incident excitation polarizing parallel to [010] direction. Thus, the crystal orientation of GeAs flake can be readily determined via angular-resolved Raman spectroscopy. To confirm the small band gap of multiplayer GeAs, we measure its Fourier-transform infrared spectra (FT-IR) (Figure S1c, Supporting Information). A sharp drop of transmission is observed starting from 1.8 µm (black curve), which confirms its absorption of mid-infrared light due to small band gap. The corresponding Tauc plot of multilayer GeAs flake is also plotted (blue line) considering an indirect transition. Optical bandgap of 0.62 eV is then estimated by extrapolation (red dashed line) of the linear region to the abscissa, the value of which is close to theoretical result.[23] Other optical characterization of GeAs has not been completed due to the unstable nature of few layer GeAs flake in the air and its indirect band gap for all thickness.

We have next carried out systematic investigation of the electronic properties of GeAs flakes. Theoretical work has reported that bulk GeAs has a calculated indirect bandgap of 0.57 eV[23] that can expand to indirect bandgap of 1.66 eV[26] when shrinking down to monolayer thickness. To characterize the electrical properties of GeAs, we fabricated back-gated field-effect transistors using multilayer GeAs flake as the channel. Because of the metastable nature of GeAs under ambient conditions, single-layer GeAs transistor on SiO_2 shows poor

© 2018 WILEY-VCH Verlag GmbH & Co. KGaA, Weinheim

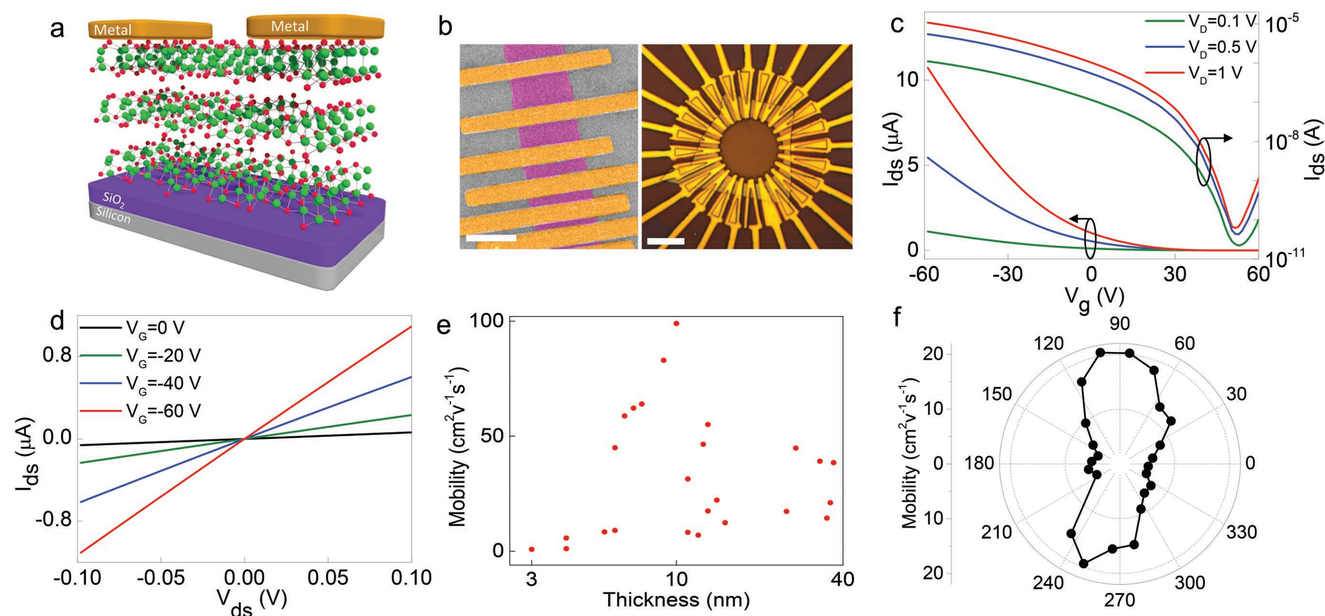

Figure 2. Electrical transport of GeAs field-effect transistors at room temperature. a) Schematics of device structure of few-layer GeAs transistor with back-gate configuration. b) The left panel is SEM image of transistor on one GeAs flake but with various channel length for TLM test. Scale bar is 3 µm. The right panel is optical image of transistors on one GeAs flake but with electrodes spaced 15° apart for angle dependent transport measurement. The scale bar is 10 µm. c) Transfer characteristics of a typical few-layer GeAs transistor at source–drain bias of 100 mV, 500 mV, and 1 V with linear axis on the left and logarithmic axis on the right. d) Output characteristics of few-layer GeAs transistor in (c) at various gate voltage. e) Hole mobility of GeAs flakes as a function of thickness. The highest field-effect mobility reaches 99 $cm^2 V^{-1} s^{-1}$ and average value is around 40 $cm^2 V^{-1} s^{-1}$. f) Polar plot of anisotropic field-effect mobility. Anisotropic ratio reaches 4.8.

electronic performance. Therefore, we focus our investigation on few-layer GeAs transistors. GeAs flakes with various thicknesses were exfoliated from the bulk crystal and then transferred onto a p^{++} silicon substrate with 300 nm thermally grown silicon oxide. After patterning contact via e-beam lithography technique, metallization was performed by evaporating 20 nm/50 nm Ni/Au on GeAs flakes. Schematics of a finished GeAs transistor is illustrated in **Figure 2**a. Left panel of Figure 2b shows a SEM image of finished GeAs transistor for transfer length method (TLM) test and right panel shows an optical image of finished GeAs transistors for angle-resolved transport measurement, which are discussed in detail below.

The transfer and output characteristics of typical few-layer (5–10 nm) GeAs transistors are first measured at room temperature under vacuum of 10^{-5} Torr. By sweeping gate voltage from 60 to −60 V, GeAs transistors are turned ON at threshold voltages of ≈−10 V (Figure 2c), indicating p-type electrical transport. Note that the ON–OFF ratio of few-layer GeAs transistors current exceeds 10^5 at room temperature at bias of 1 V, which is sufficient for typical logical electronics. With detailed investigation, we found that the ON–OFF ratio drops when body thickness becomes thicker. Specifically, multilayer GeAs transistor cannot be completely turned OFF when thickness is over 21 nm (32 layers) (Figure S2a, Supporting Information). Such thickness-dependent transfer characteristics is commonly observed in multilayer 2DSCs transistors, in which the gate electric field depletes channel region only within Debye length, so the channel region beyond Debye length remains conductive maintains high OFF current.[27] For the output characteristics (Figure 2d), linear curves are observed for most negative gate voltage, which demonstrate satisfactory Ohmic contact at room temperature. Details of the metal-GeAs contacts are discussed below.

We have next extracted the field-effect mobility via linear region of transfer curve I_D–V_G using equation $\mu = \left(\frac{1}{C_{ox}} \frac{L}{W} \frac{\partial G}{\partial V_G}\right)$, where L, W is channel length and width, C_{ox} = 11.6 nF cm^{-2} is 300 nm SiO_2 dielectric capacitance, G is channel conductance, and V_G is gate voltage. For total 25 transistors, we plot the extracted mobility as a function of thickness (Figure 2e). For thickness below 6 nm, mobilities are rather low (<10 $cm^2 V^{-1} s^{-1}$) due to unstable nature of GeAs flakes in air. Considerably higher mobility values (≈50–100 $cm^2 V^{-1} s^{-1}$) are observed in the 6–10 nm regime due to reduced impact on the surface degradation. It is also noted that mobility decreases again in thicker flakes (≈15–50 $cm^2 V^{-1} s^{-1}$ for 10–40 nm flakes), which may be attributed to electrostatic screening effect in the thick flakes, making it less sensitive to gate field and thus leading to apparently lower field-effect mobility. Similar effect was also observed in thickness dependent mobility studies in MoS_2.[28–30] It is also noted that mobility data points are scattered for a given thickness, which may be partly attributed to the highly anisotropic transport in GeAs crystals. Overall, the highest mobility reaches 99 $cm^2 V^{-1} s^{-1}$, while the average mobility is around 40 $cm^2 V^{-1} s^{-1}$. We would note the extrinsic mobility of GeAs transistor is comparable with that of typical TMDCs, e.g., MoS_2 transistors[4,31] without contact optimization or dielectric engineering.

Considering highly anisotropic nature of GeAs crystal structure and Raman spectrum, we investigated the angle-resolved transport in GeAs crystal utilizing the device geometry shown

© 2018 WILEY-VCH Verlag GmbH & Co. KGaA, Weinheim

15214095, 2018, 21, Downloaded from https://onlinelibrary.wiley.com/doi/10.1002/adma.201705934 by California Inst of Technology, Wiley Online Library on [30/12/2023]. See the Terms and Conditions (https://onlinelibrary.wiley.com/terms-and-conditions) on Wiley Online Library for rules of use; OA articles are governed by the applicable Creative Commons License

15214095, 2018, 21, Downloaded from https://onlinelibrary.wiley.com/doi/10.1002/adma.201705934 by California Inst of Technology, Wiley Online Library on [30/12/2023]. See the Terms and Conditions (https://onlinelibrary.wiley.com/terms-and-conditions) on Wiley Online Library for rules of use; OA articles are governed by the applicable Creative Commons License

in right panel of Figure 2b. The polar plot of angle dependent field-effect mobility is plotted in Figure 2f with resolution of 15°, which shows obvious anisotropic characteristics with period of 180°, coincident with periodicity of Raman spectrum. The anisotropic ratio, i.e., ratio of maximum and minimum mobility is as high as 4.8, which is comparable with black phosphorus[32] and promising for the realization of novel polarization dependent electronic and optoelectronic devices. To match the maximum mobility with crystal orientation, we plot the angle resolved Raman intensity of peak at 272 cm^{-1} and hole mobility in one polar plot (Figure S1d, Supporting Information). The orientation of polar plot also corresponds to optical image of the device in Figure 2b right panel. Specifically, each data point of Raman intensity in Figure S1d (Supporting Information) corresponds to incident excitation on Figure 2b right panel with polarization along the data point and origin point. While each data point of mobility corresponds to electrical current flowing perpendicular to the direction along data point and origin point. Since maximum value of Raman intensity and mobility in polar plot is overlapping approximately, so we infer that maximum mobility is reached when intralayer current flows perpendicular to *b* direction of GeAs crystal.

To unveil the intrinsic electronic properties of GeAs, metal and semiconductor contact, which generally dominates the electronic transport in 2DSC transistors, needs to be systematically studied and carefully excluded during analysis. Temperature dependent transport measurement gives detailed insight to electronic properties of channel material as well as contact properties. Hence, we carry out temperature dependent electrical measurement of GeAs transistors using physical property measurement system (PPMS, Quantum Design Inc.). As shown in **Figure 3**a, upon a temperature reduction for a typical few-layer GeAs transistor, the transfer curves show a transition from p-type unipolar transport to ambipolar transport. Meantime, for a typical thick GeAs transistor, transfer curves show enlarged ON–OFF ratios as well as a transition from unipolar to ambipolar transport (Figure S2b, Supporting Information). Theoretically, at low temperatures, ionization of dopants and intrinsic excitation of carriers could be suppressed. Thus, for GeAs transistors at low temperature, channel becomes more neutrally doped due to incomplete ionization of dopants and presents ambipolar transport. Meanwhile, gate tunability could be enhanced due to less populated carriers and leads to higher ON–OFF ratio. Our observation and theory are consistent with previous reports of other narrow bandgap semiconductors such as germanium.[33]

The output characteristics of typical few-layer GeAs transistors at various temperature are next studied. The I_D–V_{DS} curves (Figure 3b) at gate voltage of −60 V show noticeable nonlinearity below 50 K, which is especially obvious for short channel devices. The nonlinearity normally implies barrier limited transport, which becomes prominent at lower temperatures due to insufficient thermal energy for thermal emission. To prove our inference, we extracted effective barrier height from temperature dependent source drain current in short channel device using thermionic emission model $I_{sat} = AA^*T^2 \exp[-q\Phi/(k_BT)]$, where A is the Schottky junction area, $A^* = 4\pi qm^*k_B{}^2h^{-3}$

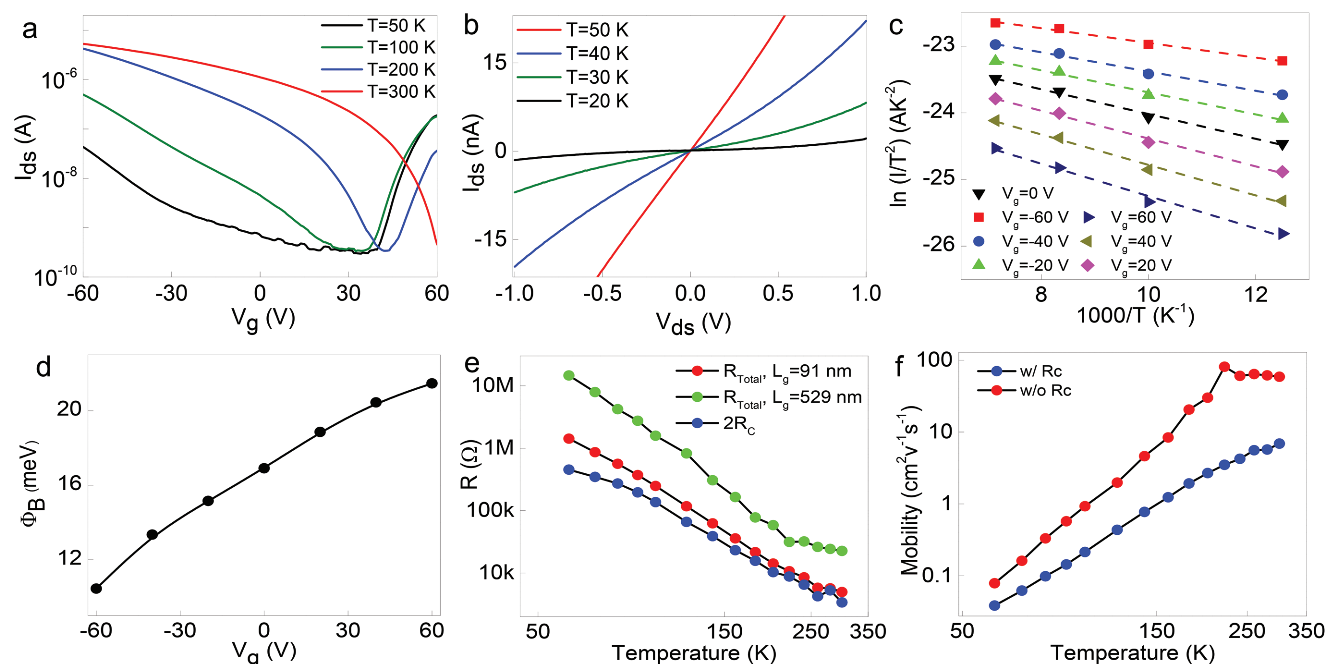

Figure 3. Temperature dependent transport of GeAs transistors. a) Transfer characteristics of few-layer GeAs transistor under various temperature. The bias voltage V_{DS} is 1 V. Ambipolar behavior is observed below 200 K. b) Output characteristics of few-layer GeAs transistor under various temperature. *I*–*V* curve shows observable nonlinearity below 50 K. c) Richardson plot of $\ln(I/T^2)$ versus 1000/T for Ni/Au and GeAs contact under various gate voltage. d) Schottky barrier height versus gate voltage extracted from fitting curves in (c). e) Temperature dependent transistor resistance (red and green dots) and contact resistance (blue curve) of few-layer GeAs transistor. The red and green dots correspond to transistors of 91 and 529 nm channel length, respectively. The R_C is extracted by transfer line method under bias and gate voltage of 0.1 and 60 V. f) Temperature dependent field-effect mobility with (extrinsic mobility) and without (intrinsic mobility) R_C.

 © 2018 WILEY-VCH Verlag GmbH & Co. KGaA, Weinheim

15214095, 2018, 21, Downloaded from https://onlinelibrary.wiley.com/doi/10.1002/adma.201705934 by California Inst of Technology, Wiley Online Library on [30/12/2023]. See the Terms and Conditions (https://onlinelibrary.wiley.com/terms-and-conditions) on Wiley Online Library for rules of use; OA articles are governed by the applicable Creative Commons License

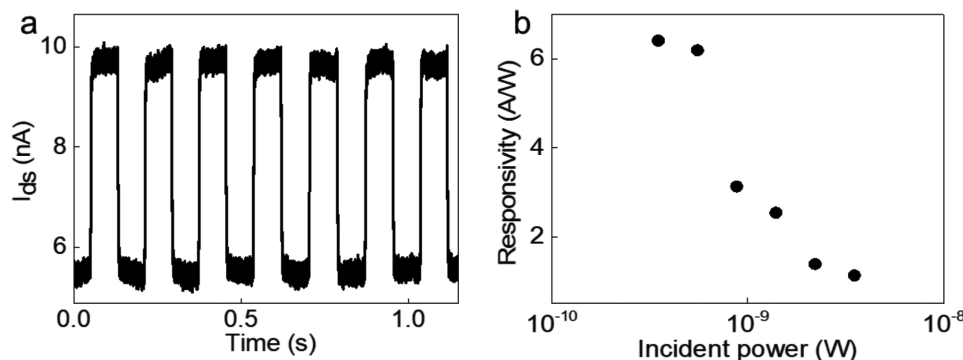

Figure 4. Photoresponse of GeAs transistor to infrared 1.6 µm laser for optical communication. a) Photoswitching behavior of GeAs transistor recorded at $V_d = 2$ V and incident power of 3.5 nW. Rise and fall time of 2.5 and 3.2 ms are determined, respectively. b) Photoresponsivity as a function of incident power at drain bias of 2 V.

is the Richardson constant, q is the elementary charge, k_B is the Boltzmann constant, T is temperature, m^* is the effective mass, and h is the Plank constant.[34] Richardson plot of $\ln(I/T^2)$ versus $1000/T$ (Figure 3c) shows negative and varied slope at different gate voltage. Effective barrier heights as function of gate voltage are then extracted (Figure 3d) from fitting data in Figure 3c. All barrier heights show positive values, ranging from 10 to 21 meV for gate voltage from −60 to 60 V. Hence, the noticeable Schottky barrier height could be the reason for inducing nonlinearity at low temperature, especially for short channel devices.

To precisely assess the intrinsic carrier mobility of GeAs transistor, we measured the temperature dependent R_C by TLM using device structure in left panel of Figure 2b, Then the intrinsic mobilities are extracted from R_C deducted transfer characteristics. Since the R_C is highly dependent on GeAs thickness, source–drain bias, and gate voltage, we choose GeAs transistor with few-layer thickness and a high ON–OFF ratio. Then total resistance is measured under fixed 0.1 V and 60 V on drain-source and gate-source terminal, respectively. The total resistance (R_T) and extracted R_C using TLM both continuously increase at low temperatures (Figure 3e), which, at first glance, indicates possible barrier limited transport as discussed above. However, after examining R_T of various channel length, we found that R_T of longer transistor (green dots in Figure 3e) is significantly higher than R_C at all temperature region. It means that R_C is only a minor portion of R_T for longer channel transistor even at low temperatures. To confirm our inference, we examined the output curves of two channel length transistors at $T = 50$ K (Figure S2c, Supporting Information). The longer transistor (red curve) exhibits near-linear output characteristics while the shorter transistor (black curve) shows obvious nonlinearity. Thus, the potential barrier from contact is not completely limiting electrical transport in relatively long few-layer GeAs transistors. To assess the intrinsic transport at low temperature, we then deducted the contact resistance from transfer characteristics (transistor corresponding to red dots in Figure 3e) and obtained the intrinsic mobility without R_C (Figure 3f). Obviously, the mobility excluding R_C is considerably higher than mobility including R_C in a wide temperature region. Thus, in this temperature region the R_C limits the transport in shorter channel transistors. At low temperature, intrinsic mobility continuously drops due to strong charged impurity scattering, which is a common limiting factor of carrier mobility at low temperatures. Similar charged impurity scattering limited transport was also reported in other defect-rich materials including 2D and traditional semiconductors.[35–37]

Narrow bandgap semiconductors can enable photoresponse to mid-infrared radiation and hence are widely utilized for optical communication. Multilayer GeAs crystal has bandgap of 0.57 eV (corresponding to 2175 nm wavelength) with photon absorption range covering the mid-infrared region. We have therefore examined photoresponse of few-layer GeAs transistor under the excitation of 1.6 µm wavelength continuous laser source. Considering the excitation wavelength is at the top end of the linear region of Tauc plot (Figure S1c, Supporting Information), absorption at 1.6 µm should not be from Urbach tail[38] of a defective semiconductor. When switching the excitation with 3.5 nW power, the output current at $V_D = 2$ V and $V_G = 60$ V was measured. The current versus time (**Figure 4**a) exhibits a relatively short rise and fall time of 2.5 and 3.2 ms, respectively. The photoresponse is limited by the bandwidth of the current meter used to measure the photocurrent. Because of the relatively low photocurrent, a high sensitivity (20 nA V^{-1}) for current meter is required, which results in small bandwidth (400 Hz) with a millisecond response time. By varying the laser power, GeAs transistor shows considerable photoresponsivity ranging from 1.13 to 6.42 A W^{-1} at $V_D = 2$ V (Figure 4b). The fast photoswitching behavior and considerable photoresponsivity of multilayer GeAs transistor at mid-infrared region enables novel 2D optoelectronics for optical communication.

To conclude, we examine the crystal structure and electrical properties of few-layer GeAs. The few-layer GeAs transistors show p-type transport with ON–OFF ratio of 10^5 and highly anisotropic field-effect mobility with maximum of 99 $cm^2 V^{-1} s^{-1}$ at room temperature. We found charged impurity scattering limits the intrinsic transport of GeAs at low temperature. Fast and intense photoresponse to mid-infrared radiation is demonstrated in multilayer GeAs transistors.

Experimental Section

Bulk GeAs was synthesized from elements via solid-state synthetic methods with a 5% excess of As added, then later sublimed off using

 © 2018 WILEY-VCH Verlag GmbH & Co. KGaA, Weinheim

a temperature gradient.[23] The as-grown crystal cleaved into shiny, reflective, mirror-like surfaces, which were then micromechanically exfoliated to obtain the GeAs flakes. The HRTEM images were captured using Titan scanning transmission electron microscopy operating at 300 kV after wet transferring GeAs flakes on TEM grids. The height profile of GeAs flakes was obtained by using atomic force microscope system (Dimension Icon). Raman spectrum studies of GeAs flakes were conducted using a confocal micro-Raman system (Horiba LABHR) excited by 633 nm laser and angle dependent Raman spectrum was obtained by precisely rotating sample orientation. FT-IR spectra were obtained with a Perkin-Elmer Spectrum instrument equipped with a universal attenuated total reflectance accessory. After preparing GeAs flakes on SiO_2/Si substrate, two-probe contacts were patterned using electron beam lithography and followed by electron beam evaporation of Ni/Au and lift-off process. Electrical measurements at room temperature were carried out in probe-station (Lakeshore, TTP4) coupled with a precise source/measurement unit (Agilent B2902A). Temperature dependent transport was studied in PPMS (Quantum Design Inc.) under 10 Torr vacuum also coupled with Agilent B2902A. Time resolved photoresponse was studied by measuring output current while chopping (7 Hz) 1.6 µm continuous mode laser beam (Santec TSL-210V) with SR570 Low-Noise Current Preamplifier with sensitivity of 20 nA V^{-1}.

Supporting Information

Supporting Information is available from the Wiley Online Library or from the author.

Acknowledgements

J.G. and Y.L. contributed equally to this work. The authors acknowledge the Nanoelectronics Research Facility (NRF) at UCLA for technical support. X.D. acknowledges financial support by ONR through grant number N00014-15-1-2368. Y.H. acknowledges the financial support from National Science Foundation EFRI-1433541. K.K. acknowledges the financial support from U.S. Department of Energy, Office of Basic Energy Sciences, Division of Materials Science and Engineering under Award DE-SC0008931.

Conflict of Interest

The authors declare no conflict of interest.

Keywords

2D semiconductors, few-layer, field-effect transistors, GeAs, infrared photodetectors

Received: October 11, 2017
Revised: January 1, 2018
Published online: April 2, 2018

[1] W. Zhang, Z. Huang, W. Zhang, Y. Li, *Nano Res.* **2014**, *7*, 1731.
[2] L. K. Li, Y. J. Yu, G. J. Ye, Q. Q. Ge, X. D. Ou, H. Wu, D. L. Feng, X. H. Chen, Y. B. Zhang, *Nat. Nanotechnol.* **2014**, *9*, 372.
[3] F. N. Xia, H. Wang, Y. C. Jia, *Nat. Commun.* **2014**, *5*, 4458.
[4] B. Radisavljevic, A. Radenovic, J. Brivio, V. Giacometti, A. Kis, *Nat. Nanotechnol.* **2011**, *6*, 147.
[5] J. K. Ellis, M. J. Lucero, G. E. Scuseria, *Appl. Phys. Lett.* **2011**, *99*, 261908.
[6] Z. Ni, Q. Liu, K. Tang, J. Zheng, J. Zhou, R. Qin, Z. Gao, D. Yu, J. Lu, *Nano Lett.* **2011**, *12*, 113.
[7] G. Fiori, F. Bonaccorso, G. Iannaccone, T. Palacios, D. Neumaier, A. Seabaugh, S. K. Banerjee, L. Colombo, *Nat. Nanotechnol.* **2014**, *9*, 768.
[8] H. Liu, A. T. Neal, P. D. Ye, *ACS Nano* **2012**, *6*, 8563.
[9] Y. Yoon, K. Ganapathi, S. Salahuddin, *Nano Lett.* **2011**, *11*, 3768.
[10] S. B. Desai, S. R. Madhvapathy, A. B. Sachid, J. P. Llinas, Q. Wang, G. H. Ahn, G. Pitner, M. J. Kim, J. Bokor, C. Hu, *Science* **2016**, *354*, 99.
[11] D. Jena, *Proc. IEEE* **2013**, *101*, 1585.
[12] A. Splendiani, L. Sun, Y. Zhang, T. Li, J. Kim, C.-Y. Chim, G. Galli, F. Wang, *Nano Lett.* **2010**, *10*, 1271.
[13] R. Yang, Z. Wang, P. X.-L. Feng, *Nanoscale* **2014**, *6*, 12383.
[14] L. Li, Y. Yu, G. J. Ye, Q. Ge, X. Ou, H. Wu, D. Feng, X. H. Chen, Y. Zhang, *Nat. Nanotechnol.* **2014**, *9*, 372.
[15] J.-H. Choi, Y.-J. Park, H.-S. Min, *IEEE Electron Device Lett.* **1995**, *16*, 527.
[16] J. Kang, W. Cao, X. Xie, D. Sarkar, W. Liu, K. Banerjee, *Proc. SPIE* **2014**, *9083*, 908305.
[17] H. Rydberg, M. Dion, N. Jacobson, E. Schröder, P. Hyldgaard, S. Simak, D. C. Langreth, B. I. Lundqvist, *Phys. Rev. Lett.* **2003**, *91*, 126402.
[18] M.-Y. Li, C.-H. Chen, Y. Shi, L.-J. Li, *Mater. Today* **2015**, *19*, 322.
[19] L. Ma, D. N. Nath, E. W. Lee, C. H. Lee, M. Yu, A. Arehart, S. Rajan, Y. Wu, *Appl. Phys. Lett.* **2014**, *105*, 072105.
[20] M. Miao, J. Botana, E. Zurek, T. Hu, J. Liu, W. Yang, *Chem. Mater.* **2016**, *28*, 1994.
[21] P. Wu, M. Huang, *Phys. Status Solidi B* **2016**, *253*, 862.
[22] J. W. Rau, C. Kannewurf, *Phys. Rev. B.* **1971**, *3*, 2581.
[23] K. Lee, S. Kamali, T. Ericsson, M. Bellard, K. Kovnir, *Chem. Mater.* **2016**, *28*, 2776.
[24] R. Blachnik, E. Irle, *J. Less Common Met.* **1985**, *113*, L1.
[25] J. Kutzner, J. Kortus, O. Patzold, U. Wunderwald, G. Irmer, *J. Raman Spectrosc.* **2011**, *42*, 2132.
[26] L. Zhou, Y. Guo, J. Zhao, *Phys. E* **2017**.
[27] S. Das, J. Appenzeller, *Phys. Status Solidi RRL* **2013**, *7*, 268.
[28] R. Cheng, S. Jiang, Y. Chen, Y. Liu, N. Weiss, H. C. Cheng, H. Wu, Y. Huang, X. Duan, *Nat. Commun.* **2014**, *5*, 5143.
[29] S. Das, H.-Y. Chen, A. V. Penumatcha, J. Appenzeller, *Nano Lett.* **2012**, *13*, 100.
[30] S.-L. Li, K. Wakabayashi, Y. Xu, S. Nakaharai, K. Komatsu, W.-W. Li, Y.-F. Lin, A. Aparecido-Ferreira, K. Tsukagoshi, *Nano Lett.* **2013**, *13*, 3546.
[31] S. Kim, A. Konar, W.-S. Hwang, J. H. Lee, J. Lee, J. Yang, C. Jung, H. Kim, J.-B. Yoo, J.-Y. Choi, *Nat. Commun.* **2012**, *3*, 1011.
[32] Y. Liu, T. Low, P. P. Ruden, *Phys. Rev. B* **2016**, *93*, 165402.
[33] W. Van Den Daele, E. Augendre, C. Le Royer, J.-F. Damlencourt, B. Grandchamp, S. Cristoloveanu, *Solid State Electron.* **2010**, *54*, 205.
[34] W. J. Yu, Z. Li, H. Zhou, Y. Chen, Y. Wang, Y. Huang, X. Duan, *Nat. Mater.* **2013**, *12*, 246.
[35] A. Prakash, Y. Cai, G. Zhang, Y. W. Zhang, K. W. Ang, *Small* **2017**, *13*.
[36] T. Zhao, W. Shi, J. Xi, D. Wang, Z. Shuai, *Sci. Rep.* **2017**, *7*, 46200.
[37] H. Ng, D. Doppalapudi, T. Moustakas, N. Weimann, L. Eastman, *Appl. Phys. Lett.* **1998**, *73*, 821.
[38] A. Hassanien, A. A. Akl, *Superlattices Microstruct.* **2016**, *89*, 153.

© 2018 WILEY-VCH Verlag GmbH & Co. KGaA, Weinheim

15214095, 2018, 21, Downloaded from https://onlinelibrary.wiley.com/doi/10.1002/adma.201705934 by California Inst of Technology, Wiley Online Library on [30/12/2023]. See the Terms and Conditions (https://onlinelibrary.wiley.com/terms-and-conditions) on Wiley Online Library for rules of use; OA articles are governed by the applicable Creative Commons License